

See discussions, stats, and author profiles for this publication at: <https://www.researchgate.net/publication/256423954>

Molecular Dynamics Simulations of Ion Conductance in Field-Stabilized Nanoscale Lipid Electropores

ARTICLE in THE JOURNAL OF PHYSICAL CHEMISTRY B · SEPTEMBER 2013

Impact Factor: 3.3 · DOI: 10.1021/jp401722g · Source: PubMed

CITATIONS

9

READS

45

4 AUTHORS:



Ming-Chak Ho

University of Southern California

9 PUBLICATIONS 33 CITATIONS

[SEE PROFILE](#)



Maura Casciola

Sapienza University of Rome

7 PUBLICATIONS 45 CITATIONS

[SEE PROFILE](#)



Zachary A Levine

University of California, Santa Barbara

26 PUBLICATIONS 197 CITATIONS

[SEE PROFILE](#)



P. Thomas Vernier

Old Dominion University

116 PUBLICATIONS 2,148 CITATIONS

[SEE PROFILE](#)

Molecular Dynamics Simulations of Ion Conductance in Field-Stabilized Nanoscale Lipid Electropores

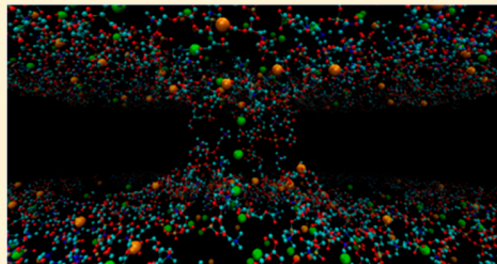
Ming-Chak Ho,[†] Maura Casciola,[‡] Zachary A. Levine,[†] and P. Thomas Vernier^{*§}

[†]Department of Physics and Astronomy, Dornsife College of Letters, Arts, and Sciences, University of Southern California, Los Angeles, California, United States

[‡]Department of Information Engineering, Electronics, and Telecommunications, University of Rome “La Sapienza”, Rome, Italy

[§]Ming Hsieh Department of Electrical Engineering, Viterbi School of Engineering, University of Southern California, Los Angeles, California, United States

ABSTRACT: Molecular dynamics (MD) simulations of electrophoretic transport of monovalent ions through field-stabilized electropores in POPC lipid bilayers permit systematic characterization of the conductive properties of lipid nanopores. The radius of the electropore can be controlled by the magnitude of the applied sustaining external electric field, which also drives the transport of ions through the pore. We examined pore conductances for two monovalent salts, NaCl and KCl, at physiological concentrations. Na^+ conductance is significantly less than K^+ and Cl^- conductance and is a nonlinear function of pore radius over the range of pore radii investigated. The single pore electrical conductance of KCl obtained from MD simulation is comparable to experimental values measured by chronopotentiometry.



1. INTRODUCTION

Electroporation, a widely used method for introducing foreign materials into cells,^{1,2} has been studied experimentally and with analytical and numerical models for decades.^{3–5} A current goal in improving our understanding of electroporation is the development of a comprehensive microscopic description of the phenomenon, not an easy task due to the nanoscale dimensions of the lipid electropore and the short time scale (nanoseconds) of pore creation, which present challenges to direct experimental observations. For these reasons, molecular dynamics (MD) simulations have become a useful tool for the study of electroporation in atomic detail. In the past decade, MD simulations have revealed many microscopic aspects of electroporation including the molecular structure of the electropore^{6–9} and the dynamics and energetics of pore creation and annihilation.^{10–12} Despite this progress, MD simulation results are rarely correlated directly and quantitatively with experiments.

A recently developed method for stabilizing electropores in MD simulations^{13,14} enables the characterization of the properties of these permeabilizing structures under controlled, steady-state conditions. The pores can be sustained for long periods (hundreds of nanoseconds or longer) by applying an external electric field of the appropriate magnitude along the axis of the pore. The diameter of the pore can be tuned by varying the external field, enabling a systematic examination of the ion conductance of lipid electropores.

Historically, an increase in electric conductance was the first indicator of the electric field-driven breakdown of the membrane barrier function that has come to be known as electroporation,^{15,16} and the measurement of conductance is

still a useful method for characterizing membrane permeabilization.¹⁷ In this paper, we compare conductance values from chronopotentiometric studies of planar lipid bilayers, which can measure the conductance of a single electropore,^{18–20} to those obtained from MD simulations of field-stabilized electropores in 1-palmitoyl-2-oleoyl-sn-glycero-3-phosphatidylcholine (POPC) bilayers in aqueous solutions containing Na^+ , K^+ , and Cl^- . The maintenance of intracellular and extracellular concentrations of these ions ($[\text{Na}^+]$ is much higher outside the cell; $[\text{K}^+]$ is much higher inside the cell) is critical for the electrophysiology of living cells. Disruption of these intracellular–extracellular ion gradients, normally maintained by ion channels and pumps at considerable energy expense,²¹ by electroporation, which allows diffusive transport of ions and small molecules through the permeabilized membrane,^{22,23} has profound consequences for the cell, which must restore osmotic and ion balance or die.

Ions affect the properties of lipid bilayers, including area per lipid, headgroup orientation, and lateral lipid mobility, as shown both experimentally and in simulations.^{24–29} MD models of ion transport through porated lipid bilayers suggest that Na^+ increases electropore line tension as a result of Na^+ -phospholipid binding, resulting in pore destabilization and a decrease in pore lifetime.³⁰ Ion transport through porated lipid bilayers has been studied to a limited extent with MD methods,^{30,31} but here we report the first molecular measurement of ion electrical conductance through electric field-

Received: February 18, 2013

Revised: August 2, 2013

Published: September 4, 2013

induced pores, and we compare these results with those obtained from experimental systems.

2. METHODS

Molecular Dynamics Simulations. All simulations were performed using GROMACS version 4.0.5³² on the University of Southern California High Performance Computing and Communications (HPCC) Linux cluster (<http://www.usc.edu/hpcc/>). Lipid topologies were taken from OPLS united-atom parameters,³³ and the Simple Point Charge (SPC) model³⁴ was used for water. For Na⁺, K⁺, Cl⁻, we employed the set of parameters originally developed by Straatsma and Berendsen³⁵ that are supplied with the GROMACS force field. All simulations were performed under the NPT ensemble. Temperature was held at 310 K with an external heat bath using a velocity rescaling algorithm³⁶ with a relaxation time of 0.1 ps. Pressure was held at 1 bar using a weak coupling algorithm³⁷ with a relaxation time of 1 ps and compressibility of 4.5×10^{-5} bar⁻¹ semi-isotropically applied in both normal and in-plane directions relative to the membrane. Bond lengths were constrained using the LINCS algorithm³⁸ for lipids and the SETTLE algorithm³⁹ for water. Short-range electrostatic and Lennard-Jones interactions were cut off at 1.0 nm. Long-range electrostatic interactions were calculated with a PME algorithm⁴⁰ using fast Fourier transforms and conductive boundary conditions. Reciprocal-space interactions were evaluated on a 0.12 nm grid with fourth order B-spline interpolation. Periodic boundary conditions in all directions were employed to mitigate system size effects.

Systems and Structures. All simulations contain a bilayer composed of 128 POPC lipids (64 per leaflet) and approximately 9000 water molecules (~70 waters/lipid), corresponding to an initial system box size of approximately 7 nm × 7 nm × 10 nm. The GROMACS function “genion” was used to replace bulk water molecules with Na⁺, K⁺, and Cl⁻. A total of 40 Na⁺ and 40 Cl⁻ were added to the NaCl system and 22 K⁺ and 22 Cl⁻ were added to the KCl system in order to create systems with free ion concentrations close to physiological values after equilibration. A custom Perl program was used to check the binding of ions to the lipid bilayer; an ion within 0.3 nm of a POPC glycerol backbone acyl oxygen is considered bound. We equilibrate the systems until the numbers of free and bound ions in the system and the area per lipid reach a steady value. Equilibration time is typically 100 ns for NaCl systems and 50 ns for KCl systems.

Conductance Simulations. Utilizing a protocol similar to the one developed by Fernández et al.¹⁴ to produce electric field-stabilized pores, we apply an external porating electric field ($E_p = 400$ MV/m) to a POPC bilayer. When the phosphorus groups from the top and bottom leaflets merge,¹² and the pore radius reaches approximately 1 nm, we reduce the external field to a lower, sustaining field ($E_s = 50, 75$, and 100 MV/m; note that these fields correspond to transmembrane potentials of roughly 200, 300, and 400 mV). Under these conditions the pore is maintained in a steady state. If ions are present in the system they are electrophoretically driven through the pore, creating an ionic current. Conductance simulations were run for 100 ns after the reduction of the external field to E_s . Three independent trials were carried out for each E_s by assigning every atom a randomized velocity (a built-in function of GROMACS) at the time the field was reduced.

In addition, we measured the electrophoretic mobility of the ions in bulk water at several ion concentrations. A simulation

box of bulk water with dimension 7 nm × 7 nm × 10 nm is created using the GROMACS function “genbox” and ions are inserted with GROMACS function genion. The system is equilibrated for 300 ps, and simulations of 5 ns with an applied external field are performed to measure the electrophoretic mobility.

Pore Radius Measurement. A custom Perl script is used to extract the radius of the electropore. The script first shifts the configuration to center the pore within the simulation box according to the water density distribution in all three dimensions. Then the upper and lower bounds of the pore region are defined using the average of the 15 largest and smallest z-coordinates of the POPC phosphorus atoms. Next the script defines a series of bins of 1.5 nm in the z-direction starting at the low boundary of the pore region. The analysis proceeds in 0.5 nm increments of the bin center plane, from the i th to the i th + 1 bin (see Figure 1). For each bin, the script

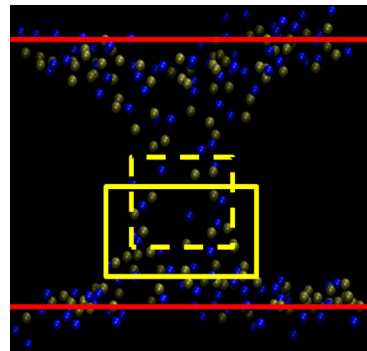


Figure 1. Pore radius measurement in a POPC electropore. Only phosphorus (gold) and nitrogen (blue) atoms are displayed for clarity. The red lines represent the boundaries of the pore region. The solid yellow box represents the i th bin and the dashed yellow box represents the i th + 1 bin at a given step of the analysis.

examines all the coordinates of the POPC nitrogen atoms and the POPC phosphorus atoms within the bin and finds the maximum and minimum x - and y -coordinates of those atoms. The x - and y -coordinates of the pore center of each bin are defined as the midpoint between the maximum and minimum values in the x - and y -directions. The pore radius of each bin is defined as the average distance in the x - y plane from the pore center to all POPC nitrogen and phosphorus atoms within the bin. At the end, the script selects the smallest radius as the pore radius at that time step. When the shape of the pore is not perfectly cylindrical, the script finds the approximate radius at the minimum point.

Current Measurement. A custom Perl script is used to extract the current from the conductance simulations. The script first defines the pore region as described above. The pore center plane is defined as the midplane between the upper bound and the lower bound of the pore region. The Perl script counts the ions of each species that cross through the center plane and divides the count by the elapsed time to obtain the current. In most cases, the current was measured for 50 ns after the pore radius reached a steady value.

Conductance Calculation. For each conductance calculation, we define the bilayer thickness as the time-averaged pore region thickness from the current measurement plus 1 nm (the water density is approximately the bulk water density at a distance of 0.5 nm beyond the pore region). The potential

across the pore is then defined as the bilayer thickness times the value of the external field. The conductance is obtained by dividing the current by the potential across the pore.

Electropore Ion Concentration Measurement. The ion concentration inside an electropore is evaluated by counting the number of ions and water molecules inside the pore region then extracted from the relation $(c_{\text{ion}}/c_{\text{water}}) = (N_{\text{ion}}/N_{\text{water}})$, where the concentration of water c_{water} is assumed to be the bulk value 55.6 M.

Images. Molecular graphics images were generated with visual molecular dynamics (VMD).⁴¹

3. RESULTS AND DISCUSSION

Ion Interactions with the Phospholipid Interface. In our simulations, Na^+ binds more strongly to the phospholipid interface than K^+ or Cl^- with bound Na^+ located deep in the interface at the acyl oxygens of the glycerol backbone and K^+ and Cl^- showing little affinity for the bilayer, consistent with previous MD studies.^{26,29} Figure 2 shows radial distribution

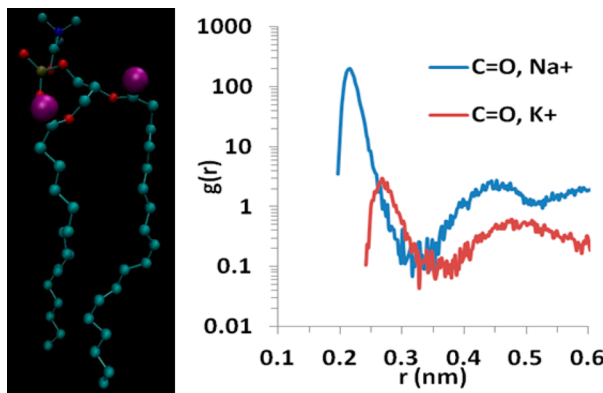


Figure 2. Left panel: snapshot of a single POPC molecule. The main ion binding sites (both glycerol backbone acyl oxygens, $\text{C}=\text{O}$) are represented by purple spheres. Right panel: radial distribution function $g(r)$ between both glycerol backbone acyl oxygens and cations. $g(r)$ is plotted on a log scale in order to display both curves.

functions for both Na^+ and K^+ with respect to the backbone $\text{C}=\text{O}$ oxygens (sn-1 and sn-2 positions are merged into one binding data set). With roughly equivalent ion concentrations in the bulk water (0.11 M Na^+ , 0.12 M K^+), the Na^+ peak is orders of magnitude higher than the K^+ peak. Figure 2 also demonstrates graphically the validity of the choice of 0.3 nm as the limiting separation for bound ions and acyl oxygens.

This Na^+-K^+ difference is known to be exaggerated by the GROMACS default parameters used in these simulations.^{26,31,42} Because the van der Waals radius (σ) of Na^+ in this model is much less than that of K^+ ($\sigma_{\text{K}}/\sigma_{\text{Na}} \approx 2.5$), an atom can approach closer to Na^+ than to K^+ , and the electrostatic attraction between a negatively charged atom or a region of high electron density and Na^+ is stronger. For other force fields, such as CHARMM⁴³ and KBFF,^{44,45} σ_{K} is much smaller than the GROMACS parameter ($\sigma_{\text{K,CHARMM}}/\sigma_{\text{K,GROMACS}} \approx 0.55$ and $\sigma_{\text{K,KBFF}}/\sigma_{\text{K,GROMACS}} \approx 0.47$). With these alternate parameters, K^+ exhibits more significant attraction to POPC and resides deeper in the membrane.^{26,42}

Pore Formation and Stabilization. In the porating external field $E_p = 400$ MV/m, an electropore appears in both NaCl and KCl POPC systems within 2 ns. In this high electric field, the pore will continue to expand until finite size

effects dominate the simulation and the bilayer becomes disorganized. To stabilize the pore, we reduce the field to a lower sustaining value E_s when the pore radius reaches approximately 1 nm. Although the choice of E_p and the target radius are somewhat arbitrary, we have shown previously that the initial configuration does not influence the steady-state properties of the electropore.¹⁴

We investigated sustaining field values $E_s = 30, 40, 50, 75, 100$, and 120 MV/m for both NaCl and KCl systems. For $E_s = 30$ MV/m, the external field failed to sustain the pore in the NaCl system (the pore annihilated within 10 ns in 2 independent trials). For $E_s = 40$ MV/m, a pore is sustained for more than 15 ns in the NaCl system, but we did not observe significant Na^+ transport during this time (probably the pore is too small) and could not obtain a reproducible ion current with this field. In KCl systems the electropore was sustained for over 15 ns at $E_s = 30$ MV/m (and also at 40, 50, 75, and 100 MV/m) in three independent trials. At $E_s = 120$ MV/m, the bilayer became disorganized within 100 ns in both NaCl and KCl systems, a result of finite size effects and the periodic boundary conditions.

For $E_s = 50, 75$, and 100 MV/m, electropores are stabilized for at least 200 ns in both NaCl and KCl systems. Figure 3 shows the evolution of the pore size after the external field is reduced to E_s . The radius (initially about 1 nm in each case) reaches a field-stabilized value within 30 ns. The stabilized, time-averaged pore radius for each E_s , calculated from the last 50 ns of each simulation for both NaCl and KCl systems, increases linearly with E_s over this range of sustaining field values (Figure 3). For a given value of E_s , the pore radius for the NaCl system is 140 pm smaller than for the KCl system, probably a result of the more extensive Na^+ binding to POPC, which decreases the area per lipid and increases the pore line tension.³⁰

Na^+ , K^+ , and Cl^- Conductance. Table 1 summarizes the electrophoretic mobilities and molar conductivities extracted from our simulations of Na^+ , K^+ , and Cl^- in bulk water. The mobility of Na^+ is less than that of K^+ and Cl^- , a consequence of the larger hydrodynamic radius of Na^+ . At infinite dilution, the ratio between the known values of K^+ molar conductivity and Na^+ molar conductivity⁴⁶ ($\Lambda_{\text{K}}^0/\Lambda_{\text{Na}}^0$) is approximately 1.5. We obtained approximately the same ratio in our simulations, ($\Lambda_{\text{K}}^0/\Lambda_{\text{Na}}^0 \approx 1.6$). At 0.15 M, the molar conductivity of ions decreases according to Kohlrausch's law. As a result of cation–anion interactions, the ratio between the molar conductivities $\Lambda_{\text{K}}/\Lambda_{\text{Na}}$ in our simulation increases to approximately 1.8.

The conductance of an electroporated lipid bilayer for a given ion species is determined by the native ion conductance, by ion-pore interactions, and by the radius of the pore, which can be tuned with the sustaining field E_s . Ion conductance increases with pore radius, as one would expect (Table 2), but Na^+ conductance is significantly less than K^+ conductance for a given radius. This is a consequence of stronger Na^+ binding to the interface, which results also in the nonlinear relation between pore radius and Na^+ conductance at small values for the pore radius (Figure 4). At $r_{\text{pore}} = 0.77$ nm (the smallest pore radius measured in the KCl system), the ratio of the cation conductances, $G_{\text{K}}/G_{\text{Na}}$, is approximately 5.6, a reflection of the stronger interaction between Na^+ and the phospholipid head groups in the pore wall relative to K^+ . At $r_{\text{pore}} = 1.5$ nm (the largest pore radius measured in the NaCl system), $G_{\text{K}}/G_{\text{Na}}$ is only 2.3. As the pore size increases, a larger and larger fraction of the sodium ions traversing the pore sees only bulklike water

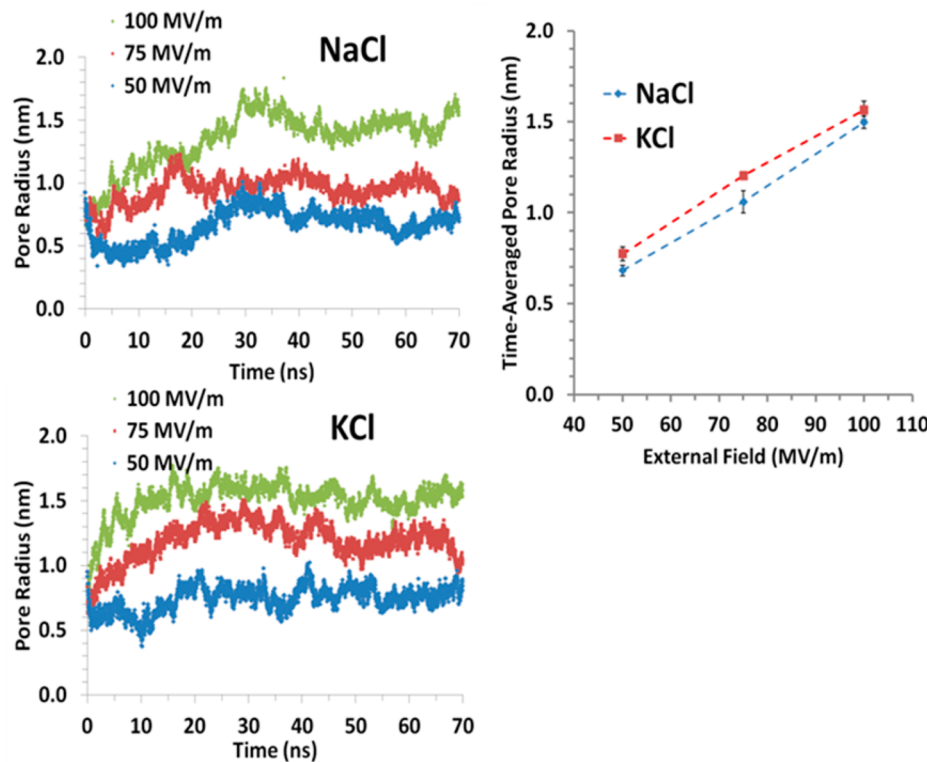


Figure 3. Left panels: Pore radius versus time from selected conductance simulations. At $t = 0$ the external field is reduced to the values in the legend. Right panel: Time-averaged pore radius versus sustaining field E_s . Results are averaged over three independent trials. Errors are given as standard deviation of the mean.

Table 1. Electrophoretic Mobilities and Conductivities in Bulk Water^a

ion	simulated electrophoretic mobility ($\text{m}^2 \text{V}^{-1} \text{s}^{-1}$)	simulated molar conductivity at 0.15 M, 310 K ($\text{S m}^2 \text{mol}^{-1}$)
Na^+	0.64×10^{-7}	6.14×10^{-3}
K^+	1.12×10^{-7}	10.78×10^{-3}
Cl^- (in NaCl)	1.01×10^{-7}	9.73×10^{-3}
Cl^- (in KCl)	1.06×10^{-7}	10.23×10^{-3}
ion	simulated limiting molar conductivity at 310 K ($\text{S m}^2 \text{mol}^{-1}$)	limiting molar conductivity at 298 K ($\text{S m}^2 \text{mol}^{-1}$) ⁴⁶
Na^+	7.7×10^{-3}	5.01×10^{-3}
K^+	12.1×10^{-3}	7.35×10^{-3}
Cl^-	11.1×10^{-3}	7.63×10^{-3}

^aElectrophoretic mobility is obtained from 5 ns of MD simulation with NVT ensemble. Simulated molar conductivity is calculated from the electrophoretic mobility.

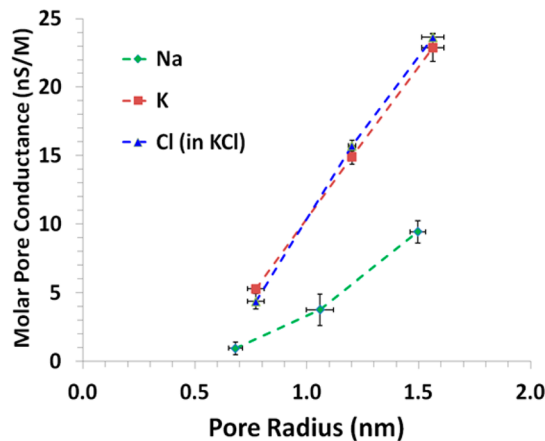


Figure 4. Ion conductance versus pore radius. Conductances of K^+ and Cl^- were obtained from the same sets of simulations.

Table 2. NaCl and KCl conductance in POPC electropores^a

system	sustaining field (MV/m)	pore radius (nm)	bilayer thickness (nm)	cation current (nA)	anion current (nA)	cation molar conductance (nS/M)	anion molar conductance (nS/M)
NaCl	50	0.68 ± 0.03	4.71 ± 0.02	0.03 ± 0.02	0.20 ± 0.03	0.95 ± 0.47	6.43 ± 0.85
	75	1.06 ± 0.06	4.87 ± 0.06	0.18 ± 0.05	1.12 ± 0.16	3.76 ± 1.15	23.17 ± 3.39
	100	1.50 ± 0.03	5.05 ± 0.07	0.63 ± 0.05	2.48 ± 0.14	9.43 ± 0.82	37.31 ± 2.28
KCl	50	0.77 ± 0.04	4.62 ± 0.01	0.18 ± 0.01	0.15 ± 0.01	5.28 ± 0.28	4.37 ± 0.56
	75	1.20 ± 0.02	4.71 ± 0.02	0.77 ± 0.03	0.81 ± 0.02	14.92 ± 0.57	15.71 ± 0.40
	100	1.56 ± 0.05	5.07 ± 0.20	1.67 ± 0.07	1.72 ± 0.04	22.87 ± 1.00	23.64 ± 0.28

^aAll results are averaged over three independent trials. Errors are the standard deviation.

and is not slowed by pore wall binding, thus the Na^+ conductance increases relative to the K^+ conductance and $G_{\text{K}}/G_{\text{Na}}$ decreases. Preliminary data shows that this ratio approaches 1.8, the value in bulk water simulations, as the pore radius increases further. K^+ and Cl^- interact very little with the pore wall; their conductances in lipid electropores are similar to those in bulk water.

To evaluate the importance of the ion model, we repeated the conductance simulations using CHARMM parameters⁴³ for K^+ (with other atoms in GROMACS parameters). Because CHARMM K^+ binds to POPC more than GROMACS K^+ , probably because of the smaller van der Waals radius of the CHARMM K^+ , we added 25 CHARMM K^+ to the system (compared to 22 GROMACS K^+) in order to achieve a similar free K^+ concentration after equilibration. The comparison between CHARMM K^+ and GROMACS K^+ conductance is presented in Figure 5. Although the attraction between POPC

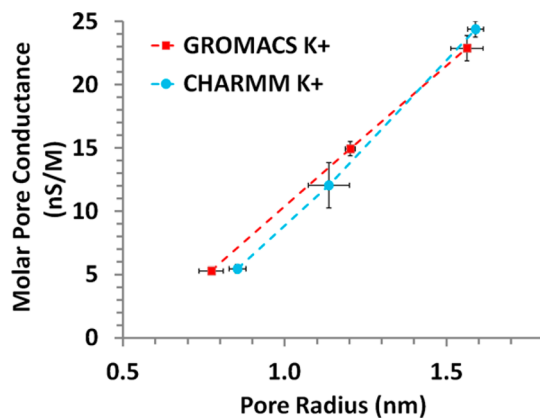


Figure 5. Molar pore conductance of K^+ using GROMACS parameters and CHARMM parameters.

and K^+ is greater using CHARMM K^+ parameters, the conductance of K^+ is only slightly lower when the pore radius is small. For a larger pore radius, the conductance for GROMACS K^+ and CHARMM K^+ is very similar.

In addition to the influence of the pore wall, interactions among the ions also affect the conductance. These interactions become more likely when the ions must pass through nanoscale pores that can exhibit selectivity and rectification.⁴⁷ In our simulations, the confinement increases the opportunity for cation–anion electrostatic attraction, which decreases the net velocity of the ions. The snapshots in Figure 6 capture this behavior. We qualitatively examined the effect of cation–anion attraction on ion transport by measuring electrophoretic mobilities in a bulk water system with varying ion concentrations. The results are summarized in Figure 7. For NaCl systems, the ion mobility decreased by nearly half when the concentration increased from about 0.1 to 1 M. For KCl systems the decrease in ion mobility is approximately 35%.

Molecular Simulations and Experimental Data. One of the goals of our study is to validate our MD simulation results by comparing them with experimental observations.^{15,16,18–20,48,49} Here we concentrate on the single-pore conductance obtained by the method of chronopotentiometry.^{18,20} Figure 8 compares conductance values from our MD simulations with those reported from chronopotentiometry experiments for POPC electropores in KCl systems. Although the two sets of conductance values lie within the same order of

magnitude, the pore radii in our simulations are smaller than those reported in the published chronopotentiometry data

There is at this time no direct method for measuring electropore radius experimentally. The pore radius values used for the chronopotentiometric results were extracted from the measured conductance using a simple model where ions are assumed to travel through the pore as they would through a cylinder of bulk water. In this model, the pore diameter²⁰ is given by $d = 2(G_p L/k\pi)^{1/2}$, where G_p is the pore conductance, L is the length of the pore, and k is the conductivity of the electrolyte. Since the accuracy of the extracted pore diameter depends on the applicability of this simple geometric model, we must place large bands of uncertainty around the chronopotentiometric results.

An additional assumption embedded in the chronopotentiometric data is that the ion concentration inside the pore is the same as it is in the electrolyte. To examine this assumption we evaluated the KCl concentration inside the electropores in our simulations (Table 3). These results show that concentrations of the confined KCl in a conducting electropore are about twice the bulk value (obtained during equilibration). Although it is not possible to say at this time which pore model is more correct, the difference in pore ion concentrations between the two models must also be taken into account when considering the correspondence between our molecular simulations and this experimental data.

Water Model. In addition to the ion model, the water model chosen for the simulations may have an effect on electropore conductance. The SPC model has been used widely in atomistic simulations of lipid bilayers, but its simplicity carries penalties. For example, the self-diffusion coefficient of SPC water is about 1.8 times higher than the known experimental value,⁵⁰ and this implies lower viscosity (based on Stokes–Einstein equation) and higher ion mobilities. In contrast, the self-diffusion coefficient of SPC/E water is about 65% of the self-diffusion coefficient of SPC water.

To examine the importance of the water model for ion conductance in our simulated electropores, we measured the velocities of single Na^+ and K^+ in bulk SPC and bulk SPC/E water (Figure 9). As expected, the electrophoretic mobility of Na^+ in SPC water is approximately 1.8 times higher than it is in SPC/E water, and the electrophoretic mobility of K^+ in SPC water is approximately 1.3 times higher than that of K^+ in SPC/E water. In conductance simulations with pores that are large enough that a significant portion of the electropore consists of bulk water, the conductance will be determined largely by the mobility of the ions in the bulk water phase. Thus as the pore radius increases, the choice of water model will have a stronger influence on the conductance.

4. CONCLUSIONS

Electrophoretic ion transport through field-stabilized lipid nanopores can be simulated using the methods of molecular dynamics. The radius of the electropore can be adjusted by varying the external field. With a bilayer system of 128 lipids and 9000 water molecules, an electropore can be stabilized with external field values from 50 to 100 MV/m, corresponding to an approximate pore radius range of 0.7 to 1.6 nm. Ion conductance is determined by two factors: pore radius and the extent of ion interaction with the phospholipid aqueous interface along the pore walls. The stronger binding of Na^+ results in significantly lower conductance for NaCl systems compared to KCl systems. This difference decreases as the pore

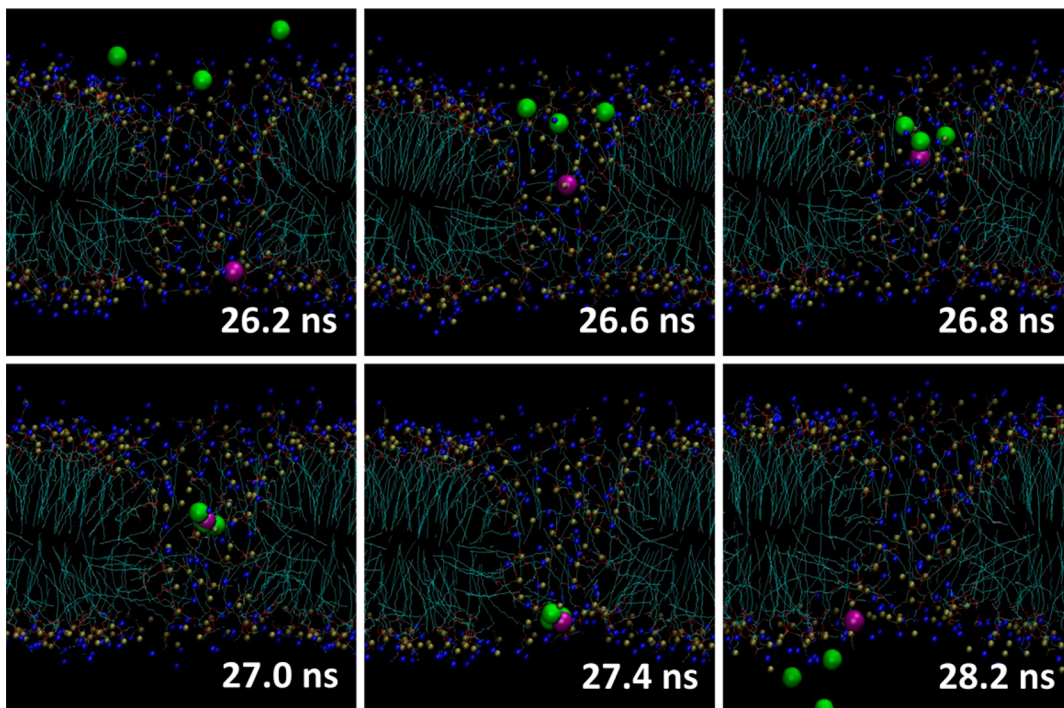


Figure 6. Ion interactions during migration through an electropore. External electric field of 75 MV/m in the $+z$ (upward) direction was applied in the snapshots. Na^+ and Cl^- ions are represented as magenta and green spheres, respectively. Phosphorus atoms and nitrogen atoms of POPC are shown as brown spheres and blue spheres to delineate the pore. Lipids tails are represented as blue lines. Water molecules and other atoms are omitted for clarity.

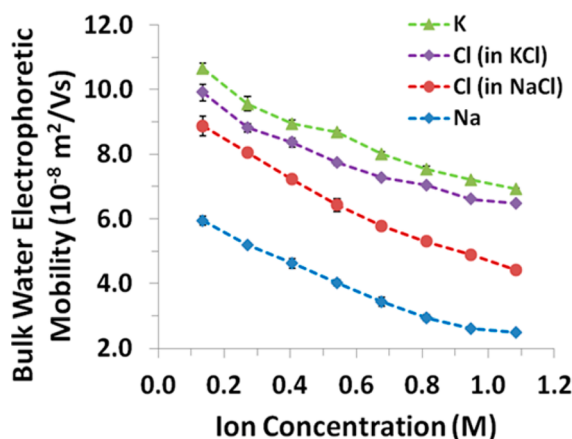


Figure 7. Simulated electrophoretic mobility of Na^+ , K^+ , and Cl^- in bulk water versus ion concentration. Each data point is the average from three independent 5 ns simulations.

radius is increased and the pore cross section becomes more and more dominated by bulk water, reducing the probability of pore wall interactions during transport. The electric conductance of a simulated electropore in a KCl-POPC system is roughly comparable to the single-pore conductance extracted from chronopotentiometric measurement, but different assumptions underlying the values used for pore radius and conductance prevent precise comparison of the two approaches. In addition, the choice of ion and water models also affects the ion conductance values extracted from simulations. Better models and new experimental methods are needed to enable quantitative comparisons between atomistic simulations and experiment.

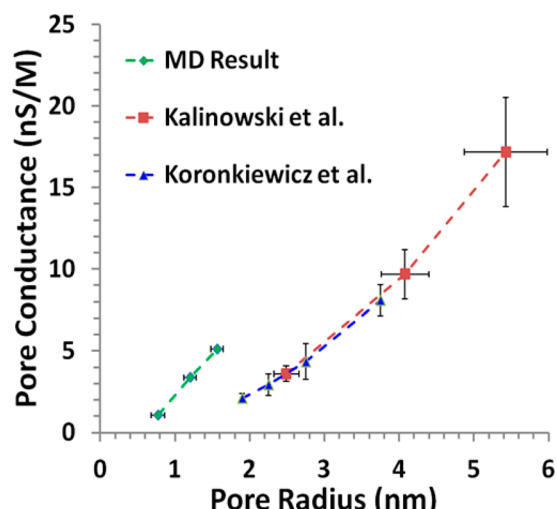


Figure 8. Comparison of simulated KCl conductance with chronopotentiometry data from Kalinowski et al.¹⁸ and Koronkiewicz et al.²⁰ Values for pore radii for the chronopotentiometric data were extracted from the conductance based on the model described in ref 20. Pore radii for MD data points were determined as described in the Methods.

Table 3. KCl Concentration Inside Electropore from MD Simulation

sustaining field (MV/m)	K^+ concentration (M)	Cl^- concentration (M)
50	0.36 ± 0.09	0.15 ± 0.02
75	0.23 ± 0.01	0.21 ± 0.01
100	0.25 ± 0.02	0.21 ± 0.02

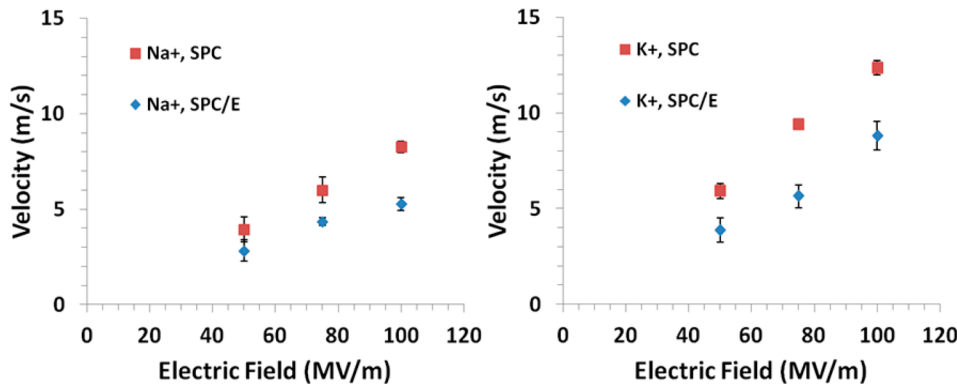


Figure 9. Velocity of single Na^+ and K^+ in SPC and SPC/E water under electric field. Each data point is the average from three independent 5 ns simulations.

AUTHOR INFORMATION

Corresponding Author

*E-mail: vernier@usc.edu.

Notes

The authors declare no competing financial interest.

REFERENCES

- (1) Teissie, J.; Golzio, M.; Rols, M. P. *Biochim. Biophys. Acta* **2005**, *1724* (3), 270–80.
- (2) Marty, M.; Sersa, G.; Garbay, J. R.; Gehl, J.; Collins, C. G.; Snoj, M.; Billard, V.; Geertsen, P. F.; Larkin, J. O.; Miklavcic, D.; et al. *EJC Supplements* **2006**, *4* (11), 3–13.
- (3) Glaser, R. W.; Leikin, S. L.; Chernomordik, L. V.; Pastushenko, V. F.; Sokirko, A. I. *Biochim. Biophys. Acta* **1988**, *940* (2), 275–87.
- (4) Weaver, J. C.; Chizmadzhev, Y. A. *Bioelectrochem. Bioenerg.* **1996**, *41* (2), 135–160.
- (5) Neu, J. C.; Krassowska, W. *Phys. Rev. E* **1999**, *59* (3), 3471–3482.
- (6) Leontiadou, H.; Mark, A. E.; Marrink, S. J. *Biophys. J.* **2004**, *86* (4), 2156–64.
- (7) Tieleman, D. P. *BMC Biochem.* **2004**, *5*, 10.
- (8) Tarek, M. *Biophys. J.* **2005**, *88* (6), 4045–53.
- (9) Vernier, P. T.; Ziegler, M. J. *J. Phys. Chem. B* **2007**, *111* (45), 12993–6.
- (10) Bockmann, R. A.; de Groot, B. L.; Kakorin, S.; Neumann, E.; Grubmuller, H. *Biophys. J.* **2008**, *95* (4), 1837–50.
- (11) Ziegler, M. J.; Vernier, P. T. *J. Phys. Chem. B* **2008**, *112* (43), 13588–96.
- (12) Levine, Z. A.; Vernier, P. T. *J. Membr. Biol.* **2010**, *236* (1), 27–36.
- (13) Piggot, T. J.; Holdbrook, D. A.; Khalid, S. *J. Phys. Chem. B* **2011**, *115* (45), 13381–8.
- (14) Fernandez, M. L.; Risk, M.; Reigada, R.; Vernier, P. T. *Biochem. Biophys. Res. Commun.* **2012**, *423* (2), 325–30.
- (15) Stampfli, R.; Willi, M. *Experientia* **1957**, *13* (7), 297–298.
- (16) Coster, H. G. *Biophys. J.* **1965**, *5* (5), 669–86.
- (17) Pakhomov, A. G.; Bowman, A. M.; Ibey, B. L.; Andre, F. M.; Pakhomova, O. N.; Schoenbach, K. H. *Biochem. Biophys. Res. Commun.* **2009**, *385* (2), 181–6.
- (18) Kalinowski, S.; Ibron, G.; Bryl, K.; Figaszewski, Z. *Biochim. Biophys. Acta, Biomembr.* **1998**, *1369* (2), 204–212.
- (19) Koroniewicz, S.; Kalinowski, S.; Bryl, K. *Biochim. Biophys. Acta, Biomembr.* **2002**, *1561* (2), 222–229.
- (20) Koroniewicz, S.; Kalinowski, S. *Biochim. Biophys. Acta* **2004**, *1661* (2), 196–203.
- (21) Armstrong, C. M.; Hille, B. *Neuron* **1998**, *20* (3), 371–80.
- (22) Pucihar, G.; Kotnik, T.; Miklavcic, D.; Teissie, J. *Biophys. J.* **2008**, *95* (6), 2837–48.
- (23) Saulis, G.; Satkauskas, S.; Pranaviciute, R. *Anal. Biochem.* **2007**, *360* (2), 273–281.
- (24) Binder, H.; Zschornig, O. *Chem. Phys. Lipids* **2002**, *115* (1–2), 39–61.
- (25) Garcia-Manyes, S.; Oncins, G.; Sanz, F. *Biophys. J.* **2005**, *89* (3), 1812–26.
- (26) Gurtovenko, A. A.; Vattulainen, I. *J. Phys. Chem. B* **2008**, *112* (7), 1953–62.
- (27) Vacha, R.; Siu, S. W. I.; Petrov, M.; Bockmann, R. A.; Barucha-Kraszewska, J.; Jurkiewicz, P.; Hof, M.; Berkowitz, M. L.; Jungwirth, P. *J. Phys. Chem. A* **2009**, *113* (26), 7235–43.
- (28) Vacha, R.; Jurkiewicz, P.; Petrov, M.; Berkowitz, M. L.; Bockmann, R. A.; Barucha-Kraszewska, J.; Hof, M.; Jungwirth, P. *J. Phys. Chem. B* **2010**, *114* (29), 9504–9.
- (29) Jurkiewicz, P.; Cwiklik, L.; Vojtiskova, A.; Jungwirth, P.; Hof, M. *Biochim. Biophys. Acta* **2012**, *1818* (3), 609–16.
- (30) Leontiadou, H.; Mark, A. E.; Marrink, S. J. *Biophys. J.* **2007**, *92* (12), 4209–15.
- (31) Gurtovenko, A. A.; Vattulainen, I. *Biophys. J.* **2007**, *92* (6), 1878–90.
- (32) Hess, B.; Kutzner, C.; van der Spoel, D.; Lindahl, E. *J. Chem. Theory Comput.* **2008**, *4* (3), 435–447.
- (33) Berger, O.; Edholm, O.; Jahnig, F. *Biophys. J.* **1997**, *72* (5), 2002–13.
- (34) Berendsen, H. J. C.; Postma, J. P. M.; van Gunsteren, W. F.; Hermans, J. In *Intermolecular Forces*; Pullman, B., Ed.; Reidel: Dordrecht, The Netherlands, 1981; pp 331–342.
- (35) Straatsma, T. P.; Berendsen, H. J. C. *J. Chem. Phys.* **1988**, *89* (9), 5876–5886.
- (36) Bussi, G.; Donadio, D.; Parrinello, M. *J. Chem. Phys.* **2007**, *126* (1), 014101.
- (37) Berendsen, H. J. C.; Postma, J. P. M.; van Gunsteren, W. F.; DiNola, A.; Haak, J. R. *J. Chem. Phys.* **1984**, *81*, 3684–3690.
- (38) Hess, B.; Bekker, H.; Berendsen, H. J. C.; Fraaije, J. G. E. M. *J. Comput. Chem.* **1997**, *18* (12), 1463–1472.
- (39) Miyamoto, S.; Kollman, P. A. *J. Comput. Chem.* **1992**, *13* (8), 952–962.
- (40) Essmann, U.; Perera, L.; Berkowitz, M. L.; Darden, T.; Lee, H.; Pedersen, L. G. *J. Chem. Phys.* **1995**, *103* (19), 8577–8593.
- (41) Humphrey, W.; Dalke, A.; Schulten, K. *J. Mol. Graphs* **1996**, *14* (1), 33–8 27–8.
- (42) Klasczyk, B.; Knecht, V. *J. Phys. Chem. A* **2011**, *115* (38), 10587–95.
- (43) Beglov, D.; Roux, B. *J. Chem. Phys.* **1994**, *100* (12), 9050–9063.
- (44) Weerasinghe, S.; Smith, P. E. *J. Chem. Phys.* **2003**, *119* (21), 11342.
- (45) Klasczyk, B.; Knecht, V. *J. Chem. Phys.* **2010**, *132* (2), 024109.
- (46) Vanýsek, P. *CRC Handbook of Chemistry and Physics*, 74th ed.; Lide, D. R., Ed.; CRC Press: Boca Raton, FL, 1993, pp 5–90.
- (47) Pakhomov, A. G.; Pakhomova, O. N. *Advanced Electroporation Techniques in Biology and Medicine*; CRC Press: Boca Raton, FL, 2010; pp 188–190.

- (48) Hibino, M.; Shigemori, M.; Itoh, H.; Nagayama, K.; Kinosita, K., Jr. *Biophys. J.* **1991**, *59* (1), 209–20.
- (49) Pavlin, M.; Kanduser, M.; Rebersek, M.; Pucihar, G.; Hart, F. X.; Magjarevic, R.; Miklavcic, D. *Biophys. J.* **2005**, *88* (6), 4378–90.
- (50) Mark, P.; Nilsson, L. *J. Phys. Chem. A* **2001**, *105*, 9954–9960.